# Deformation measurements of smart aerodynamic surfaces

Gary A. Fleming and Alpheus W. Burner

National Aeronautics and Space Administration
Langley Research Center
Hampton, Virginia 23681-2199 USA

## ABSTRACT

Video Model Deformation (VMD) and Projection Moiré Interferometry (PMI) were used to acquire wind tunnel model deformation measurements of the Northrop Grumman-built Smart Wing tested in the NASA Langley Transonic Dynamics Tunnel. The F18-E/F planform Smart Wing was outfitted with embedded shape memory alloys to actuate a seamless trailing edge aileron and flap, and an embedded torque tube to generate wing twist. The VMD system was used to obtain highly accurate deformation measurements at three spanwise locations along the main body of the wing, and at spanwise locations on the flap and aileron. The PMI system was used to obtain full-field wing shape and deformation measurements over the entire wing lower surface. Although less accurate than the VMD system, the PMI system revealed deformations occurring between VMD target rows indistinguishable by VMD. This paper presents the VMD and PMI techniques and discusses their application in the Smart Wing test.

**Keywords:** Video Model Deformation, Projection Moiré Interferometry, VMD, PMI, Smart Wing, shape memory alloy, SMA, twist

## 1. INTRODUCTION

Adaptive wings whose shape can be changed to achieve optimal aircraft performance throughout the flight envelope have been studied since the beginning of manned flight. Even the Wright flyer implemented *wing warping*, the invention considered to enable the success of the historic 1903 flight, for aircraft stability and control.[1] Integration of an adaptive, or *smart* wing in more modern aircraft has been hampered by mechanical complexity, cost, and weight penalties offsetting the net performance gain of such a device. However, smart materials such as piezoelectrics and shape memory alloys (SMAs) are offering a gateway to a fully adaptive wing with seamless control effectors. Hingeless, contoured control surfaces can provide improved aerodynamic performance over their conventional rigid counterparts. When deployed, conventional control surfaces give rise to discontinuous boundaries along the wing. These discontinuities cause early flow separation, resulting in reduced lift and increased drag. Smooth, continuous control surfaces delay the onset of flow separation and improve lift and stall angle characteristics.[2,3]

Several research programs conducted in recent years have been dedicated to development of adaptive wings for high performance aircraft.[3-5] Most recently, the joint DARPA/AFRL/NASA Smart Wing Program, led by researchers at Northrop Grumman Corporation (NGC), has explored the use of smart structures technology to achieve active wing twist and seamless control effectors. Phase I of the program produced a 16 percent scale F18-E/F planform Smart Wing with embedded SMAs to actuate seamless trailing edge control surfaces[6] and generate wing twist[7]. The Smart Wing underwent two series of wind tunnel tests in the NASA Langley (LaRC) Transonic Dynamics Tunnel; the first in May, 1996[8], and the second in July, 1998[9]. Accurate, in-situ measurement of the Smart Wing shape and deformation during these developmental wind tunnel tests was critical in understanding relationships between control surface actuation and aerodynamic reaction. Various internal and external measurement techniques for obtaining the required deformation measurements were attempted during both wind tunnel entries. The external measurement techniques, however, proved to be more accurate and reliable.[9] A LaRC-developed optical Video Model Deformation (VMD) system based on single camera / single view photogrammetry was used as the primary Smart Wing deformation measurement tool during both wind tunnel entries. A single component Projection Moiré Interferometry (PMI) system with full field measurement capability was also used during the second wind tunnel entry to complement the more accurate VMD system. This paper summarizes the use of the VMD and PMI systems for model deformation measurements during the second wind tunnel entry of the Smart Wing Phase I Program.

# 2. DEFORMATION MEASUREMENT TECHNIQUES

VMD and PMI are the two primary non-contacting optical techniques currently under development at LaRC for in-situ measurement of wind tunnel model deformation. VMD is more mature than PMI for production wind tunnel testing, having been used in nearly 20 wind tunnel tests at 5 NASA facilities since January 1996. Although LaRC-developed PMI systems have recently been used for fixed wing and rotorcraft tests in NASA facilities, the technology is not yet ready for production testing. Both techniques are video-based, but provide different types of information. VMD provides highly accurate streamwise/vertical scalar position measurements of discrete targets placed on the model from which wing twist, bending, and angle-of-attack (AoA) can be calculated. A single component PMI system provides full-field, image-based measurements of out-of-plane model shape and deformation, typically referenced to a horizontal plane at the mean vertical elevation of the model. At the current state of development, VMD measurements generally have greater absolute accuracy than PMI measurements, but PMI has the unique ability to resolve deformations occurring over the entire model surface within the field-of-view. PMI systems can therefore resolve deformations that may be unseen by VMD systems, e.g. deformations occurring in regions between VMD target locations. Both systems were used in the Smart Wing Program second wind tunnel entry to provide both highly accurate (VMD) and full-field (PMI) deformation measurements of the Smart Wing.

## 2.1 Video Model Deformation (VMD)

VMD development was initiated in the 1980s [10], based on earlier successful wind tunnel tests conducted in the 1970s using film cameras[11]. The introduction of image processing routines in the mid-1990s for automating data acquisition and reduction was a major breakthrough for VMD, facilitating near routine use in production wind tunnels[12]. The development of a commercial, target-tracking version of VMD is discussed in reference 13. A recent review of VMD can be found in reference 14.

The VMD technique consists of a single camera, single view, photogrammetric solution from digital images of targets placed on the wing at known semispan locations, figure 1. Except for these targets, which may have some minor effects on the aerodynamic data, the technique is non-intrusive. The basic hardware consists of a standard video-rate CCD video camera, light source (usually located as close to the camera as possible), frame grabber board, and computer with image acquisition and reduction software. The camera is positioned to the side and somewhat above or below the model, resulting in an oblique view of the model. Targets are typically placed on or near the fuselage to serve as controls in addition to the targets at known semispan locations along the wing. Flat black paint is sometimes used to remove glints and to increase target contrast. Image processing is used to automatically locate and compute corrected image plane coordinates for each of the targets. Single view photogrammetry is then used to determine the $X$ (streamwise), $Z$ (vertical) coordinates in object space, given the known $Y$ (crossflow) coordinates. Vertical displacements at specified chordwise locations and slope angles are computed by least squares regression for each semispan station along the wing.

The VMD system resolution depends on the fraction of the image field that the targets occupy. For cases in which the row of targets span nearly the entire image plane, sub 0.01° resolution is possible in the laboratory. Wind tunnel AoA tests using body targets indicate 0.01° resolution can be achieved during wind-off tests and is possible for wind-on tests, provided the target row(s) occupy nearly the entire image plane and model translations while changing pitch are not excessive. However, the fraction of the image plane occupied by a target row near the wing tip may be less than 25 percent in order to also image the inboard portions of the wing and body. Thus a typical angular resolution for model deformation measurements may be 0.05° or worse near the wing tip due to the small fraction of the image plane occupied by the row of targets at the tip.

The image processing techniques used in the VMD approach consist of blob analysis to locate targets, simple threshold removal, and centroiding to determine image plane coordinates in pixels. These routines can be executed at near-video rates, making the technique very amenable to online data reduction. In some cases, deformation data can be available within a few minutes of completing a set of runs, i.e. ensembles of data points acquired at varying model and/or tunnel conditions. Other systems using VMD technology compute the angle and Z-displacement as each data point is taken. Twist and bending are computed after angle correction and referencing to the wind-off polar(s) at the conclusion of a set of runs. The reduced data are then transferred to the tunnel data acquisition system (DAS) for merging with standard tunnel data.

## 2.2 Projection Moiré Interferometry (PMI)

PMI is an optically simple, non-contacting measurement technique used since the 1970s for surface topology and shape characterization[15]. The fundamentals of PMI are well known[16,17], but only recently have PMI and similar systems been used to quantitatively measure wind tunnel model deformations while under aerodynamic load. PMI development for wind tunnel model deformation measurements is described in references 14, 18, and 19.

Conventional PMI relies on the projection of a grid of equispaced, parallel lines onto the wind tunnel model surface. A raw PMI data image with perspective distortion removed is shown in figure 2. Any incoherent light source providing adequate illumination levels can be used for grid line projection. A pulsed laser diode bar emitting in the near infrared is often used for wind tunnel testing because it allows lights-on tunnel operation without sacrificing grid line contrast and provides the high illumination levels required to measure large fields-of-view. The emission linewidth of most laser diode bars renders any speckle undetectable. A Ronchi ruling (a binary grating of parallel lines having equal spacing and thickness) installed in the projector system is the physical element generating the projected grid lines. Surface preparation is generally not required for non-metallic models, but polished metal models may require painting to obtain a diffuse scattering surface. A CCD camera with a narrow bandpass filter matched to the projector illumination wavelength is positioned to view the model off-axis. Images of the grid lines projected onto the model are acquired in reference (wind-off) and loaded (wind-on) conditions using a frame grabber installed in a PC-compatible computer. Image processing routines are then used to remove camera perspective distortion and interfere the acquired images with a computationally generated reference grid, resulting in interferograms containing moiré fringes. These fringe patterns are further processed offline to obtain a quantitative, spatially continuous representation of the model surface shape or deformation[18]. The current PMI image processing software can process a single image in approximately 20 seconds on a 400 MHz Pentium II-class PC. On-line data processing is not feasible at these rates, but key datasets can be processed overnight. Efforts are currently under way to reduce the data processing time. It is believed that a factor of 4 improvement can be achieved by time optimizing the code and by using the multimedia acceleration capabilities available in modern PC processors.

PMI system resolution is primarily dependent on the video camera field-of-view, optical modulation transfer function, and illumination/observation angles. Deformation measurement resolutions better than 0.05-mm have been attained with conventional laboratory systems using 640-x 480-pixel video cameras with a 300-x 300-mm field-of-view. Absolute deformation measurement accuracies for similar laboratory systems have been shown to be better than 0.15-mm over a 50-mm range of deformations[20], equating to angular uncertainties better than 0.05°. Scaling these accuracy and resolution values to a 1.2-x 1.2-meter field-of-view representative of a large wind tunnel application, an absolute accuracy of 0.75-mm and 0.25-mm deformation measurement resolution is estimated.

# 3. EXPERIMENT

## 3.1 Smart Wing installation in the LaRC Transonic Dynamics Tunnel

The NASA Langley Transonic Dynamics Tunnel (TDT) is a closed loop, continuous return tunnel with a 4.9-x 4.9-meter test section. The tunnel can operate at Mach numbers ranging from 0.1 to 1.2, and can provide varying total pressures ranging from near vaccum to atmosphere. Originally designed for aeroelastic research, the facility can either use air or R134A gas as the test medium. The R134A gas, having a density much greater than air, facilitates wind tunnel model aeroelastic scaling. A complete description of the tunnel may be found in reference 21.

The semispan Smart Wing was a 16 percent scale F18-E/F planform wing with a 950-mm span. Figure 3 shows the Smart Wing installed in the LaRC TDT. The wing was mounted on a splitter plate extending approximately 1 meter from the tunnel wall. This moved the Smart Wing closer to the tunnel centerline, where air flow was more uniform. A large spindle protruded through the splitter plate to the tunnel wall, connecting the Smart Wing to the LaRC Semi-Span Turntable System for AoA adjustment. A five-component balance system was used to record the aerodynamic forces and moments. Air was used as the test medium in all Phase I Smart Wing Program testing.

The Smart Wing was outfitted with three smart material based control surface actuation systems: (1) A series of SMA tendons for actuation of an outboard trailing edge aileron, (2) A series of SMA tendons for actuation of an inboard trailing

edge flap, and (3) an SMA torque tube for generating wing twist. The SMA tendons were bonded to the external wing surface near the juncture of the flap/aileron with the main element. The torque tube was mounted internal to the wing and ran spanwise at approximately 50 percent chord. The primary model deformation measurements of interest were actuated flap and aileron deflection angle, and spanwise wing twist induced by torque tube actuation. VMD and PMI measurements were also desired to indicate the presence of other wing deformations potentially caused by aerodynamic loading.

The Smart Wing lower surface was painted rust red to accommodate the VMD and PMI instruments. Optimal VMD target contrast can be achieved by painting the model black, so the VMD camera views the bright targets on a black background. However, PMI projected grid line contrast is minimized when viewing black surfaces, making the acquisition of accurate measurements more difficult. Laboratory investigations revealed that rust red provided adequate scattered light (800 nm wavelength) for PMI measurements while maintaining near-maximum VMD target contrast.

## 3.2 VMD instrumentation for Smart Wing test

A standard video-grade CCD camera with 752-x 240-pixels per field was used for the VMD camera. The camera was located in a lower fillet of the test section wall, viewing the Smart Wing model through the same port as the PMI camera. Installation of the VMD and PMI cameras is shown in figure 4. The window normally covering the port housing the cameras was removed for this test. The VMD camera used a 35-mm focal length C-mount video lens to image the Smart Wing so that the targets placed on the wing remained in the field-of-view over the test AoA range. Images from the camera were digitized using a frame grabber installed in a Pentium-class PC.

The VMD targets were 19.0-mm diameter patches of retroreflective tape adhered to the model. Retroreflective targets provide high contrast imagery that greatly simplifies and increases the robustness of the image processing routines required to locate the target positions within the image plane to sub-pixel accuracy. The targets used were 0.1-mm thick with 5.0-micron rms surface roughness. Target rows were located on the turntable pitching mechanism to establish an independent optical measurement of AoA and to serve as a reference for the other target rows. Target rows were placed at a normalized semispan of 0.227, 0.612, and 0.856 on the main element of the wing, flap, and aileron. This allowed determination of the change in wing twist caused by aerodynamic loading or torque tube actuation. Targets fixed to the flap and aileron were used to measure their deflection angles. The VMD system had the ability to acquire time-dependent deflection data at 30 Hz rates to examine torque tube and flap/aileron actuation response times.

Calibration of the VMD measurement system consisted of several steps. After the proper viewing angle was established, a special 3-D calibration fixture with targets placed at known coordinates was positioned to nearly fill the camera field-of-view. Two image sequences were acquired with a known translation of the calibration fixture between the two sequences. These image sequences were then iteratively processed to determine lens radial and decentering distortion parameters and the photogrammetric principal distance. The resulting calibration coefficients are often referred to as the camera *interior orientation*. The calibration fixture was next aligned to the test section coordinate system and a single image sequence was recorded. This image sequence and the previously determined interior orientation values were used to establish the camera Euler angles and location. The final calibration stage consisted of acquiring in-situ, wind off VMD measurements of varied model AoA to calibrate the VMD system against the tunnel AoA accelerometer. This step was typically done before and after a run series to account for system changes in time and verify system stability. Although the VMD system fundamentally measures target positions in the streamwise and vertical directions, the system is best suited and most reliable for angle measurements due to these in-situ angle calibrations.

## 3.3 PMI instrumentation for Smart Wing test

The Smart Wing Phase I Program second wind tunnel entry was the first time a PMI system had been used in the TDT. The PMI projection system used for the test is shown in figure 5. A 20-Watt, 800 nm broadband laser diode bar was used as the projector illumination source. Light emitting from the laser was collected by a cylindrical lens and directed to back-illuminate a 79 line/cm Ronchi ruling. The ruling was placed at the image plane of a standard 50-mm F/1.4 SLR camera lens, whose focus was adjusted to sharpen the grid line projection on the wing. A 75-mm diameter mirror, coated for maximum reflection in the near infrared, was positioned in front of the projector lens to direct the projected grid pattern vertically upward. The entire optical system was mounted directly underneath the TDT test section floor and aligned to project the grid lines through the tunnel centerline flow expansion slot, illuminating the underside of the Smart Wing. The projected grid line pitch in the plane of the wing was 11.65-mm.

The PMI system camera was a generic RS-170 analog video camera electronically shuttered to 1/250 second. The short exposure time essentially froze the model position, so observed grid lines were not blurred under dynamic model conditions. Laser illumination was synchronized with the camera such that the laser would only emit light during the camera open shutter period. Pulsing the laser, rather than continuous operation, reduced heat load on the laser diode and ensured its survivability in the 45-degree Celsius wind tunnel operating environment. The camera was fitted with a 12.5 - 70-mm C-mount zoom lens and a precision narrowband interference filter matched to the laser emission wavelength. As discussed in section 3.2, the PMI camera was mounted alongside the VMD camera in a port located in the tunnel wall/floor fillet, figure 4. A frame grabber installed in a 200 MHz Pentium-class computer digitized images from the camera at 640-x 240-pixels per field at up to 15 Hz rates.

Calibration of the PMI system began by installing a flat 1.2-x 1.2-meter aluminum honeycomb panel in place of the Smart Wing. The rigidity of the honeycomb panel, in conjunction with a custom built support mechanism, prevented panel sag. One side of the panel contained an array of black dots (approximately 30-x 30) painted on a white background on 63.5-mm centers. The side containing the dots was placed facing downward as shown in figure 6 and illuminated with the PMI projector with the Ronchi ruling removed. Images of the dot card were digitized and processed to determine image dewarping parameters necessary to computationally remove the video camera optical and perspective distortions. Following acquisition of the dot card images, the calibration plate was turned over so the opposing side, painted flat white, faced downward. The Ronchi ruling was reinstalled in the projector, and images of the calibration plate at angles-of-attack ranging from –6 to +6° were acquired. These data were later processed to obtain an image-based deformation sensitivity calibration for the instrument.

## 4. RESULTS

Approximately 2000 tunnel data points were acquired during the test, including points acquired during calibration sequences, data runs, and repeat points. VMD deformation data of the Smart Wing were acquired for nearly all of the 2000 tunnel data points. PMI data were acquired for a selected set of 500 points. The VMD and PMI systems acquired data simultaneously, but did not have synchronized video cameras. Real-time VMD data was available throughout the test for continuous feedback to the test engineers. VMD data acquisition was more automated than PMI data acquisition since the VMD system was networked with the tunnel DAS and was triggered each time a tunnel data point was taken. The VMD and PMI systems will be networked with the tunnel DAS for future tests, facilitating hands-off data acquisition and merging of the optical data with standard DAS data. Data acquisition times for both instruments were 1 to 2 seconds per tunnel data point. Both instruments functioned nearly flawlessly throughout the tunnel entry.

The ability of PMI to quantitatively measure wing shape over the entire field-of-view is demonstrated in figure 7. The image shown in figure 7a is a greyscale representation of the Smart Wing bottom surface shape relative to the flat calibration reference panel at 0° AoA. Measurement values from single columns of pixels at 45-, 65-, and 85-percent span have been extracted from the image and plotted as line plots in figure 7b. Airfoil design data provided by NGC is also plotted for comparative purposes. The PMI wing shape measurements match the airfoil design data well, having an rms error less than 0.75-mm over the full surface of the wing. This is in agreement with the estimated accuracy values for a PMI system with a 1.2-x 1.2-meter field-of view. A systematic error in the PMI data may be seen by examining the difference between the PMI measured wing shape and airfoil design data. This difference is caused by the AoA of the wing differing slightly from the 0° AoA setting of the calibration plate when the data were acquired. The rms shape measurement error may approach 0.5-mm if this effect were removed.

Wind-off AoA sweeps performed prior to the start of the test indicated the VMD system measured model AoA to an accuracy of 0.005° rms based on independent in-situ angle measurements using a calibrated precision accelerometer. Figure 8 presents comparative VMD and PMI AoA measurements acquired during a wind-on AoA sweep at Mach 0.20 and dynamic pressure of 0.03 atm. The PMI measurements are in very close agreement with those obtained by VMD, generally within 0.05° from –4 to +10° AoA. Error bars plotted on the chart represent the AoA rms measurement precision calculated from AoA measurements at 18 independent spanwise locations along the wing. The average value of this uncertainty for the entire dataset was 0.06°. Systematic errors begin to significantly influence the data for negative AoAs exceeding –4°, reaching a maximum magnitude of 0.44° at –10° AoA. Similar trends have occurred in other datasets acquired at higher Mach numbers. An increase in PMI system AoA measurement error with increasing angle is somewhat expected, but the fact that

these systematic errors only significantly influenced negative AoAs less than –4° remains to be explained. The accuracy of the PMI system in the –4 to +10° range, however, is very encouraging.

VMD and PMI-measured aileron deflection angles acquired during a wind-on tunnel run at Mach 0.25 and 0.042-atm dynamic pressure are shown in figure 9. The ability of the VMD and PMI systems to obtain accurate aileron deflection angle measurements was compromised by the short, ~100-mm aileron chord. Laboratory investigations conducted with a foam model of identical size and planform of the Smart Wing indicated the VMD system was capable of acquiring aileron deflection angles to within 0.03° rms precision, but potentially suffered from bias errors as large as 0.25°. The data presented in figure 8 indicates there are both bias and sensitivity differences between the instruments. Once the average bias difference of 0.50° is removed, the VMD and PMI system aileron deflection angle measurements generally agree to within 0.1° through the –2 to +2° range. Larger discrepancies occur with increasing angle, reaching magnitudes of 2.5° at an approximate –9.5° deflection angle. The sensitivity difference is likely explained by the way the aileron deflection angle is calculated for the VMD and PMI systems. The VMD system, unable to detect aileron curvature, included curvature effects when calculating the aileron deflection angle. In contrast, deflection angles were calculated from the PMI results only where the aileron had a linear deflection profile, beginning approximately 40-mm from the trailing edge extending to the trailing edge. This method of processing would naturally produce higher deflection angle readings for the PMI system than for the VMD system.

VMD and PMI both have the ability to acquire time-dependent deformation data. This capability was exercised only for VMD during the Smart Wing test because of its near real-time output capability. Figure 10 shows the change in aileron deflection angle as a function of time after deactivation of the SMA tendons. Three data series are presented at +8, 0, and at a repeat point of +8° wing AoA. The data in figure 10 indicates that aileron deflection decays exponentially with a 7.0 second time constant after deactivation, and that near complete relaxation of the aileron to an equilibrium state requires at least 30 seconds. The data also illustrates the capability of VMD to obtain dynamic data, and its consistency in measurement at the three AoAs shown. Similar data were acquired to investigate flap, aileron, and torque tube actuation response times.

Results from the SMA torque tube actuation investigations were some of the most interesting obtained during the Smart Wing test. The SMA torque tube, embedded within the wing running spanwise at approximately 50 percent chord, was used to generate spanwise wing twist. The torque tube could only be actuated at off, low, and high settings. Fine adjustment of the amount of actuation was not possible. Figure 11 shows wind-on PMI-measured wing shape at 0° AoA for (a) a reference condition, and (b) a low torque tube actuation case at Mach 0.25 and a dynamic pressure of 0.04 atm. In addition to the expected wing twist, the PMI data revealed an unexpected bump in the wing that was not indicated by the VMD system. The bump was caused by the Smart Wing skin stretching over an internal structural member as the wing was twisted. Figure 12 shows the PMI-measured airfoil profiles at 85 percent span for the reference and torque tube actuated conditions. The differential wing twist is also plotted. PMI measurement values along single columns of pixels at 85 percent span were extracted from the images in figure 11 to construct the plot. Wing twist and the presence of the bump are clearly apparent, shown both in the torque tube actuated and differential wing twist profiles. The bump was unnoticed by the VMD system because it acquires deformation measurements only at the discrete target locations on the wing, and a majority of the bump occurs between target rows. Although the PMI system has lower accuracy than VMD, the data presented in figures 11and 12 clearly illustrates the merits of the PMI full-field measurement capability.

Figure 13 shows the spanwise wing twist profile for low and high torque tube actuation cases for the Smart Wing at Mach 0.20 and a dynamic pressure of 0.03-atm. The VMD-measured local wing twist is plotted for the three rows of targets on the main wing body. The PMI results show a non-linear spanwise twist distribution with a dramatic in increase in twist at 70 percent span, particularly for the high torque tube actuation case. This location corresponds to the discontinuity in the Smart Wing planform delineating the inboard and outboard sections of the wing. The discrepancy between PMI and VMD-measured wing twist is likely due to the method used to calculate the localized twist. VMD twist measurements were calculated by performing a linear regression of the streamwise/vertical coordinates of the 3 targets affixed to the wing main element in each of the three target rows. PMI measurements were calculated by performing a linear regression using measurement values from each pixel in the localized differential wing twist profile (approximately 350 points) similar to that shown in figure 12. Target locations affected by the bump in the wing, figures 11 and 12, will have greater statistical weighting in the regression of VMD data than the regression of PMI data, and will thus indicate twist angles higher than those calculated from PMI results. Because of the bump in the wing and the lack of a third means of measurement of spanwise twist, there is no way to determine which optical instrument was more accurate in representing the true spanwise twist distribution.

## 5. CONCLUSIONS

The combined use of VMD and PMI has proven to be an extremely valuable tool for wind tunnel model deformation measurements. The Smart Wing test allowed both of these techniques to showcase their best attributes. VMD remains the instrument of choice when the highest accuracy AoA, wing bending, and wing twist measurements of conventional models are required. VMD accuracy limits for AoA measurement during the Smart Wing test approached those of precision accelerometers. PMI measurements are highly applicable to models that may undergo complex deformations, such as the Smart Wing, and can indicate deformations not seen by VMD. PMI measurement accuracy levels for the Smart Wing test were better than anticipated, particularly for this first test of the system in the LaRC TDT. Continued PMI development will be directed toward removal of known systematic errors and improved calibration methods to further reach the quantitative accuracy limits characteristic of VMD. Both instruments performed nearly flawlessly throughout wind tunnel testing, but VMD is decisively more mature and amenable to production tests. PMI will undergo further enhancements to reduce data processing and analysis time leading to an instrument that can readily be used for production testing. VMD and PMI will continue to be used for the future Smart Wing Program Phase II tests. Data fusion of the PMI and VMD measurements is planned to exploit and merge the best characteristics of both techniques, producing a complete dataset of model deformation with the highest quality possible.

## 6. ACKNOWLEDGEMENTS

*Smart Wing* is a DARPA/AFRL/NASA jointly funded program. The authors wish to thank the Northrop Grumman Smart Wing Test Team and the LaRC TDT staff for accommodating the needs required to obtain the VMD and PMI measurements. The authors would also like to recognize Kenneth Cate, Harriett Dismond, Hector Soto, and Scott Bartram for their assistance and dedication in acquiring the VMD and PMI measurements.

## 7. REFERENCES

1. B. A. Haber, *The National Air and Space Museum*, Smithmark Publishing, Inc., New York, 1995. pp. 14.
2. Kudva, J. N., et al., "Overview of Recent Progress on the DARPA / USAF Wright Laboratory 'Smart Materials and Structures Development – Smart Wing' Program", SPIE Vol. 3044, 1997. pp. 24-32.
3. Kudva, J. N. et al., "Overview of the DARPA/AFRL/NASA Smart Wing Program", Paper No. 3674-26, presented at the SPIE Symposium on Smart Structures and Materials, SPIE Vol. 3674, Newport Beach, CA, March 1-4, 1999.
4. Hall, J. M., "Executive Summary AFTI/F-111 Mission Adaptive Wing", WRDC-TR-89-3083, September 1989.
5. Pendelton, E., et al., "A Flight Research Program for Active Aeroelastic Wing Technology", AIAA Paper 96-1574, presented at the 37th AIAA SDM Conference, Salt Lake City, UT, April 15-17, 1996.
6. Martin, C. A., et al., "Design and Fabrication of Smart Wing Model and SMA Control Surfaces", Paper No. 3674-27, presented at the SPIE Symposium on Smart Structures and Materials, SPIE Vol. 3674, Newport Beach, CA, March 1-4, 1999.
7. Jardine, A. P., et al., "Improved Design and Performance of the SMA Torque Tube for the Smart Wing Program", Paper No. 3674-29, presented at the SPIE Symposium on Smart Structures and Materials, SPIE Vol. 3674, Newport Beach, CA, March 1-4, 1999.
8. Scherer, L. B., et al., "Smart Wing Wind Tunnel Test Results", SPIE Vol. 3044, 1997. pp. 56-66.
9. Scherer, L. B., et al., "DARPA/AFRL/NASA Smart Wing Second Wind Tunnel Test Results", Paper No. 3674-28, presented at the SPIE Symposium on Smart Structures and Materials, SPIE Vol. 3674, Newport Beach, CA, March 1-4, 1999.
10. Burner, A. W., Snow, W. L., and Goad, W. K., "Model Deformation Measurements at a Cryogenic Wind Tunnel Using Photogrammetry", 31st ISA Symposium, San Diego, CA, May 1985; published in Instrumentation in the Aerospace Industry - vol. 31 ISA pp. 615-622.
11. Brooks, J. D. and Beamish, J. K., "Measurement of Model Aeroelastic Deformations in the Wind Tunnel at Transonic Speeds Using Stereophotogrammetry", NASA TP 1010, Oct. 1977.
12. Burner, A. W. and Martinson, S. D., "Automated Wing Twist and Bending Measurements Under Aerodynamic Load", presented at the 19th AIAA Advanced Measurement and Ground Testing Technology Conference, AIAA 96-2253, June 17-20, 1996.
13. Liu, T., Radeztsky, R., Garg, S., and Cattafesta, L., "A Videogrametric Model Deformation System and its Integration with Pressure Paint", AIAA paper 99-0568, 1999.

14. Burner, A. W., “Model Deformation Measurements at NASA Langley Research Center”, Presented at the RTO (formerly AGARD) Symposium on Advanced Aerodynamic Measurement Technology, Sponsored by NATO 22 – 25 September 1997, Seattle, Washington, NATO CP-601, May, 1998, pp. 34-1 to 34-9.
15. Patorski, K., *Handbook of the Moiré Fringe Technique*, Elsevier Science Publishers, 1993. pp. vii - xi.
16. Pirodda, L., “Shadow and projection moiré techniques for absolute or relative mapping of surface shapes”, *Optical Engineering* **21**(4), pp. 640 - 649, July/August 1982.
17. *Selected Papers on Optical Moiré and Applications*, SPIE Milestone Series, Vol. MS 64, 1992. Indebetouw, G., and Czarnek, R., editors.
18. Fleming, G. A., and Gorton, S. A., “Measurement of Rotorcraft Blade Deformation using Projection Moiré Interferometry”, Presented at the Third International Conference on Vibration Measurements by Laser Techniques, Ancona, Italy, June 16-19, 1998. SPIE Vol. 3411, pp. 514-527.
19. Fleming, G. A., and Soto, H. L., “Development of Projection Moiré Interferometry Systems for Large Wind Tunnel Applications”, to be presented at the SAE 1999 World Aviation Congress and Exposition, San Francisco, CA, October 19-21, 1999.
20. Pryputniewicz, E. J., *Development of PMI Systems for Characterization of Load-Resisting Structures*, Major Qualifying Project, Worcester Polytechnic Institute, Worcester, MA, 1999.
21. “The NASA Langley Transonic Dynamics Tunnel”, NASA LWP-799, September, 1969.

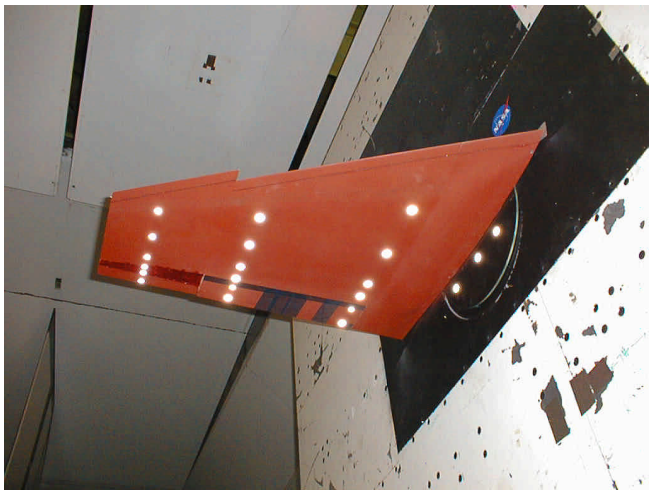

***Figure 1***: NGC Smart Wing with VMD targets at 22.7-, 61.2-, and 85.6-percent span.

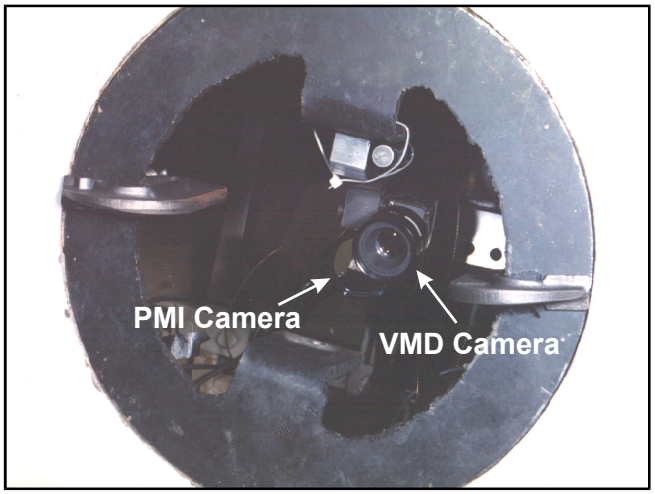


***Figure 4***: VMD and PMI camera installation in tunnel wall fillet port

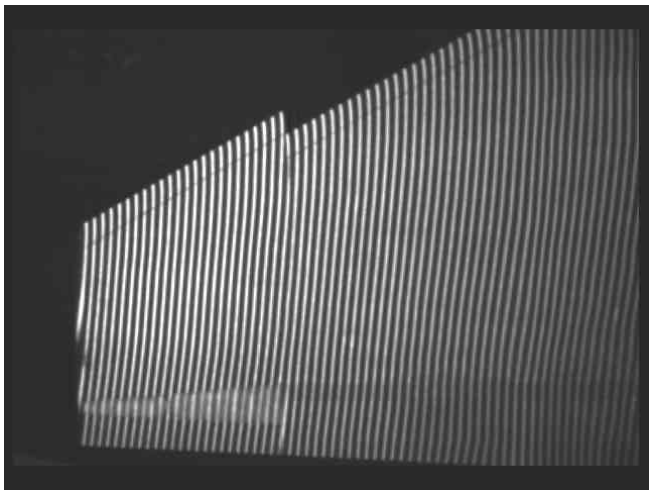

***Figure 2***: Raw PMI data image showing grid lines projected onto the Smart Wing bottom surface

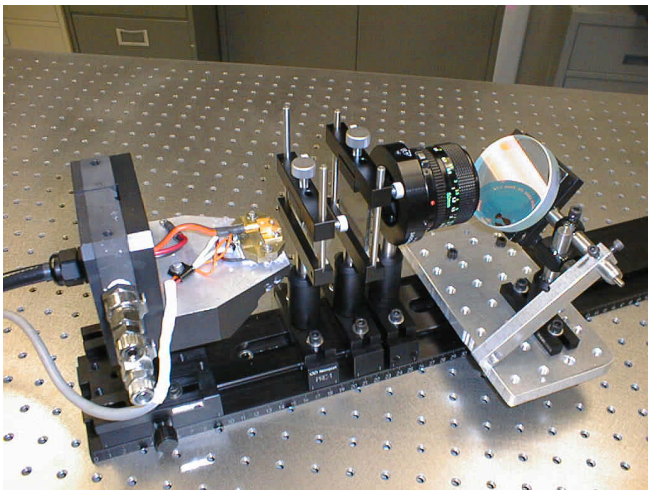

***Figure 5***: Laser diode-based PMI projector system

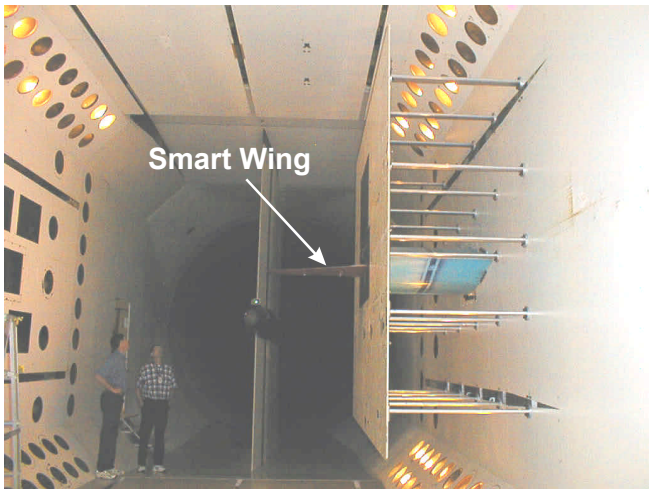


***Figure 3***: Smart Wing installation in the NASA Langley Transonic Dynamics Tunnel

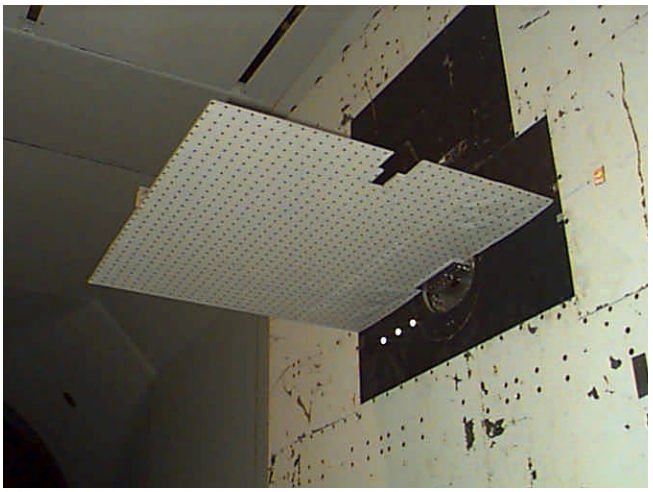

***Figure 6***: PMI calibration plate mounted in place of the Smart Wing. Dots used for camera perspective distortion removal are visible.

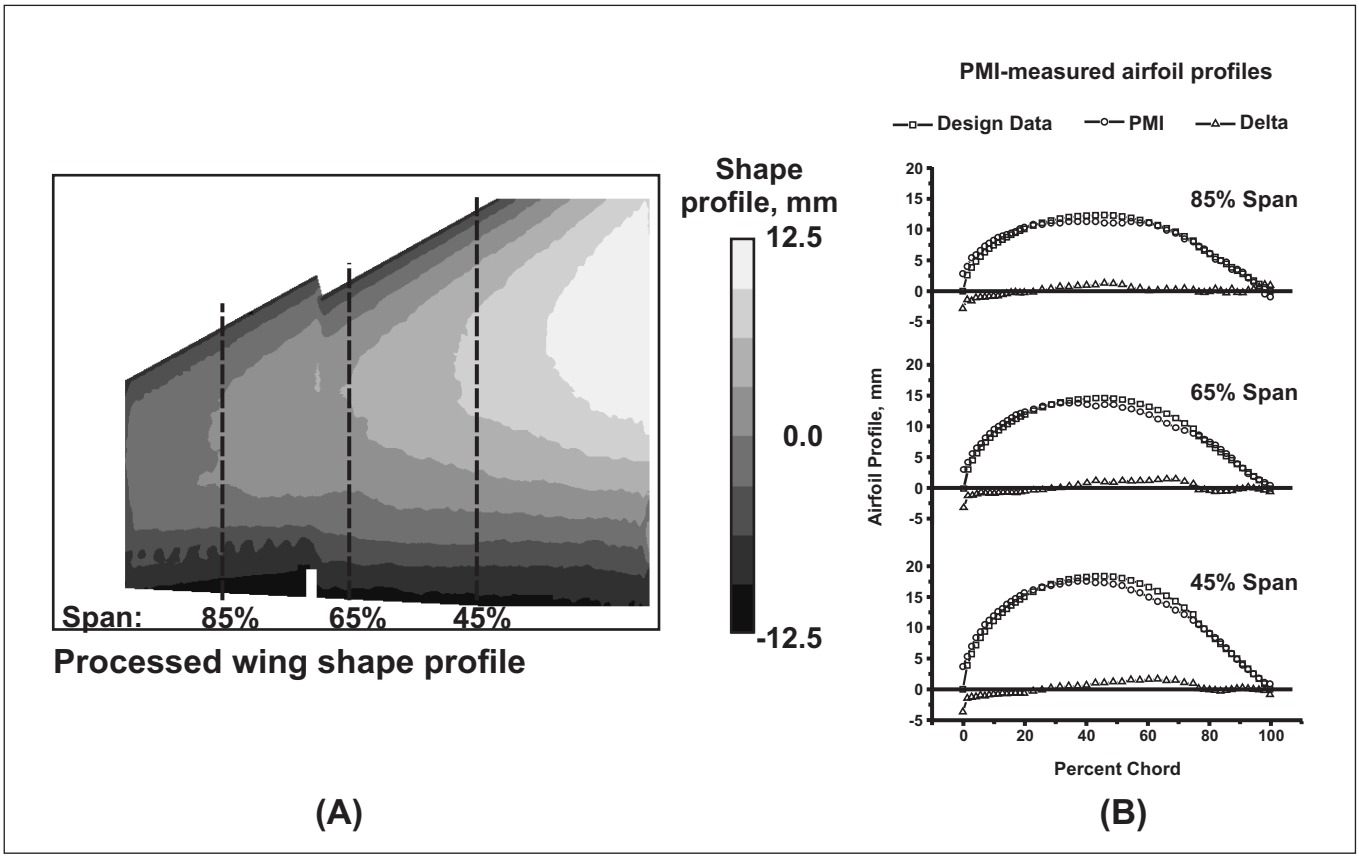


*Figure 7*: PMI-measured Smart Wing shape at 0 deg. AoA, (a) processed wing shape data, (b) airfoil profiles at 45-, 65-, and 85-percent span

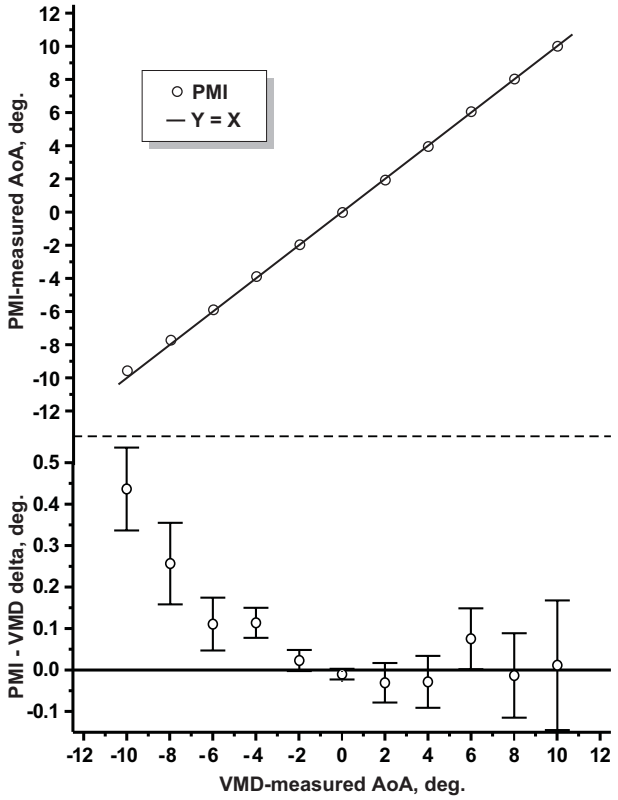


*Figure 8*: Comparative results between VMD and PMI AoA measurements

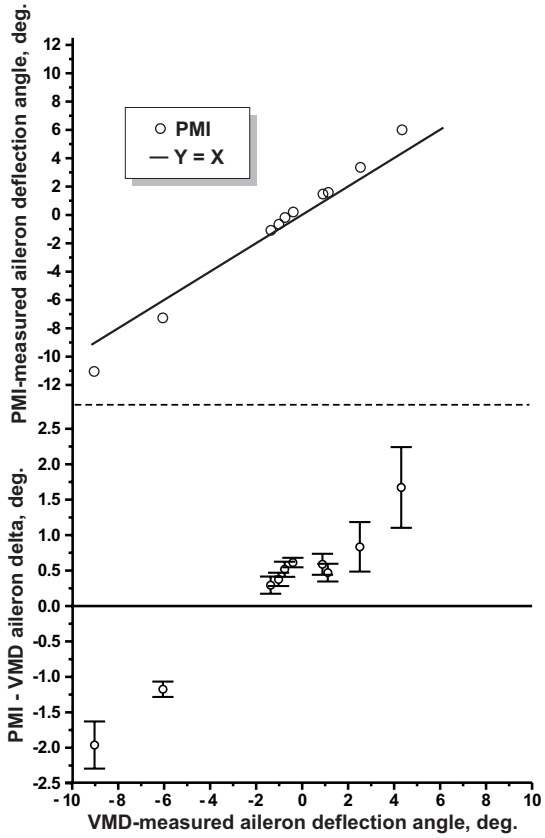


*Figure 9*: Comparative results between VMD and PMI aileron deflection angle measurements

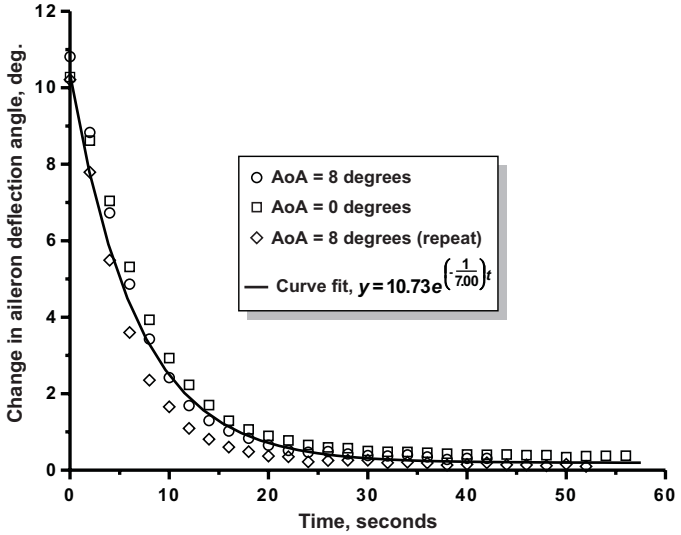


***Figure 10***: VMD-measured SMA aileron relaxation time after deactivation.

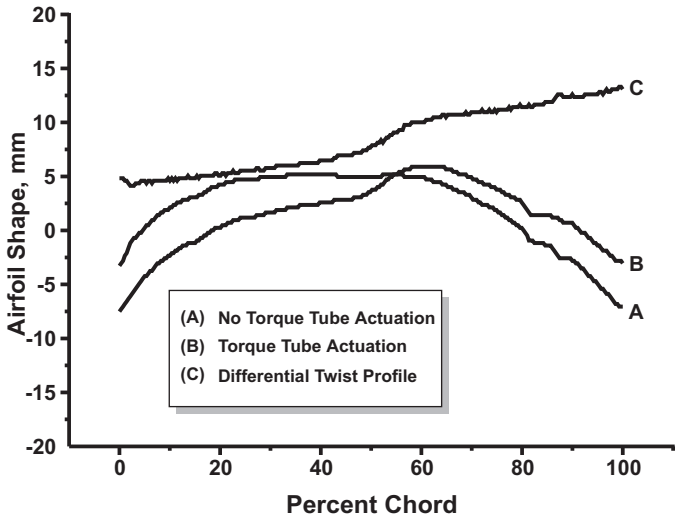


***Figure 12***: Smart Wing airfoil profiles at 85 percent span extracted from images in figure 11. Torque tube induced deformations are apparent.

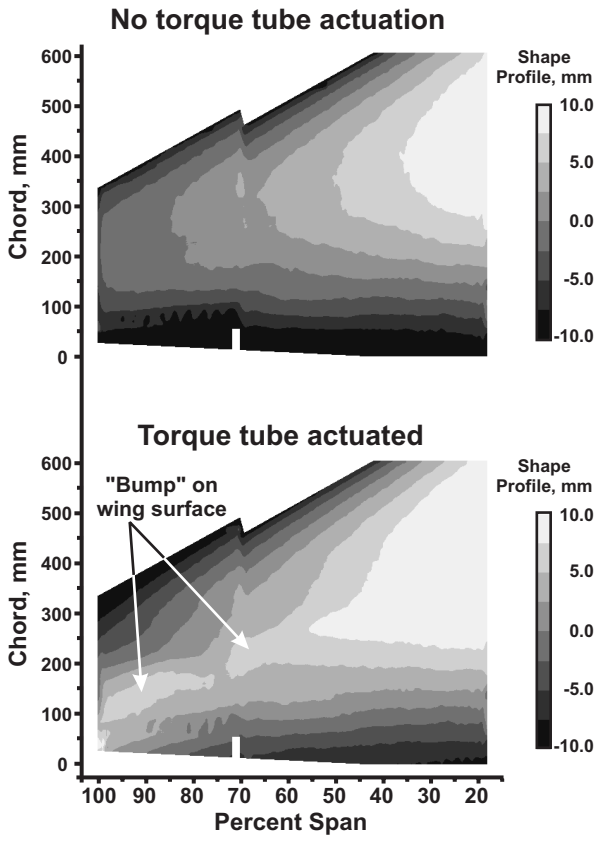


***Figure 11***: PMI-measured Smart Wing deformation caused by torque tube actuation.

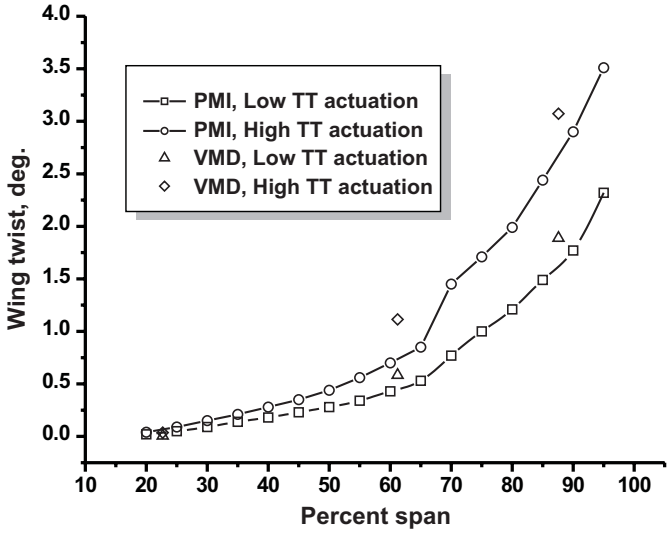


***Figure 13***: VMD and PMI Spanwise wing twist distribution measurements.